Near-infrared tandem organic photodiodes for future application in artificial retinal implants

ADVANCED MATERIALS
www.advmat.de

Near-Infrared Tandem Organic Photodiodes for Future Application in Artificial Retinal Implants

Giulio Simone, Dario Di Carlo Rasi, Xander de Vries, Gaël H. L. Heintges, Stefan C. J. Meskers, René A. J. Janssen, and Gerwin H. Gelinck**

Photovoltaic retinal prostheses show great potential to restore sight in patients suffering from degenerative eye diseases by electrical stimulation of the surviving neurons in the retinal network. Herein, organic photodiodes (OPDs) sensitive to near-infrared (NIR) light are evaluated as photovoltaic pixels for future application in retinal prostheses. Single-junction and tandem OPDs are compared. In the latter, two nominally identical single-junction cells are processed on top of each other, effectively doubling the open-circuit voltage (V_{OC}). Both single-junction and tandem OPD micropixels can deliver the required charge to stimulate neurons under pulsed NIR light at physiologically safe intensities when connected to stimulating microelectrodes in a physiological saline solution. However, only tandem OPD pixels can cover the entire charge per pulse neural stimulation window due to their higher V_{OC} (≈1.4 V). This demonstrates the viability of high-resolution retinal prostheses based on flexible OPD arrays.

Retinal degenerative diseases lead to blindness due to progressive loss of photoreceptor cells, which are responsible for the conversion of light entering the eye into electrical signals delivered to the brain. Retinitis pigmentosa and age-related macular degeneration are two leading causes of severe visual losses in adult individuals, affecting over one million people worldwide.[1,2] In patients suffering from these diseases, rod and cone photoreceptor cells are progressively lost while neural cells in the retinal network remain functional. Electronic retinal prostheses have great potential to restore sight by electrical stimulation of the surviving neurons. Over the past few years, different types of retinal implants have been investigated, mainly epiretinal and subretinal. Epiretinal implants[3] electrically stimulate the ganglion cells in the inner limiting membrane. Although they were proven to partially restore functional vision, they require complex intraocular implantation procedures. Subretinal prostheses[4] aim at the stimulation of bipolar cells in the inner nuclear layer. This approach involves simpler implantation methods and preserves the natural image-processing mechanism of the retinal network. However, additional implanted electronics is necessary to transfer power and data to the implant. To overcome this limitation, the concept of photovoltaic neural stimulation has been proposed.[5,6] In this approach, a photovoltaic implant converts the incoming light into electrical input which triggers neural activity. Photovoltaic retinal prostheses are self-powered devices which do not require any additional implanted electronics. Furthermore, they enable the preservation of the natural coupling between eye movement and image perception.

Ghezzi et al. recently developed a fully organic subretinal prosthesis based on a photoactive polymer as interface for neural stimulation.[7,8] The implant was proven to restore light sensitivity and spatial acuity in Royal College of Surgeons rats, a widely studied animal model of retinitis pigmentosa.[9] The absence of stimulating metal electrodes in this work is intriguing. The activation of the neural circuitry was ascribed to the interaction of photoexcited states in the polymeric film with the retinal environment, but the exact mechanism of neurostimulation remains uncertain.

Mathieson et al. successfully demonstrated a photovoltaic subretinal prosthesis based on silicon photodiode (Si-PD) micropixels.[5] In this system, the image captured by a head-mounted camera is processed by a portable computer and projected onto the subretinal implant from video goggles using pulsed near-infrared (NIR) (880–915 nm) light, which selectively targets the artificial prosthesis being invisible to remaining photoreceptors. Upon illumination with NIR light, pulsed photocurrent is generated in each Si-PD pixel and delivered to nearby nerve cells through stimulating microelectrodes.[10] Charge injection into the biological tissue is maximized using photovoltaic pixels

G. Simone, D. Di Carlo Rasi, X. de Vries, G. H. L. Heintges, Dr. S. C. J. Meskers, Prof. R. A. J. Janssen, Prof. G. H. Gelinck
Molecular Materials and Nanosystems
Institute of Complex Molecular Systems
Eindhoven University of Technology
P.O. Box 513, 5600 MB Eindhoven, The Netherlands
E-mail: r.a.j.janssen@tue.nl; g.h.gelinck@tue.nl
Prof. R. A. J. Janssen
Dutch Institute for Fundamental Energy Research
De Zaale 20, 5612 AJ Eindhoven, The Netherlands
Prof. G. H. Gelinck
Holst Centre
TNO-The Dutch Organization for Applied Scientific Research
High Tech Campus 31, 5656 AE Eindhoven, The Netherlands
The ORCID identification number(s) for the author(s) of this article can be found under https://doi.org/10.1002/adma.201804678.

DOI: 10.1002/adma.201804678

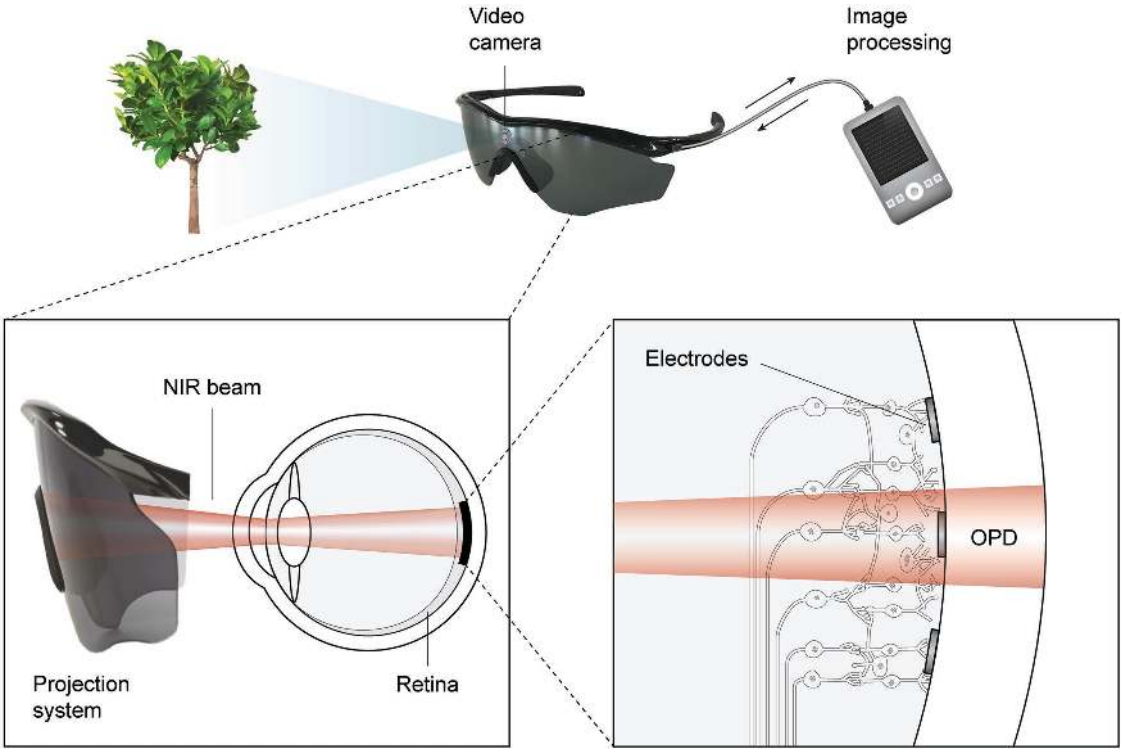

Figure 1. Concept of photovoltaic retinal implant based on NIR-sensitive OPDs. The system diagram is inspired by the seminal work of Mathieson et al.[5] The image captured by a head-mounted camera is processed by a portable computer and projected onto the subretinal implant via a near-to-eye projection system using pulsed NIR light. The OPD array converts incoming light into pulsed photocurrent that is delivered to nearby nerve cells by stimulating microelectrodes.

with three diodes in series that can increase the open-circuit voltage (V_{OC}) up to 1.5 V. Due to the brittleness of individual silicon pixels, the implant is provided with trenches in the attempt to improve flexibility.[11]

Recent advances in the field of organic electronics have led to the development of organic photodiodes (OPDs) on thin flexible substrate[12] with responsivity in the NIR range.[13] Herein, we evaluate NIR-sensitive OPDs as a possible alternative to the fully inorganic photodiodes described in the seminal work of Mathieson et al. The OPD pixel array may be processed on ultrathin plastic foil, resulting in a mechanically flexible, softer implant that responds to pulsed NIR illumination (**Figure 1**). As in the Si-PD case, photogenerated charge is delivered to the biological tissue through stimulating microelectrodes. This stimulation mechanism is well studied and makes it possible to reliably calculate the photogenerated charge once the properties of the photodiode and stimulating electrode are established. Further, the organic diodes can be stacked in the vertical direction resulting in tandem OPDs with higher V_{OC}. Vertical monolithic stacking of OPD pixels represents a potential advantage over series connected Si pixels because it enables the enhancement of the V_{OC} without increasing the pixel size, thereby maintaining high spatial resolution. The concept of tandem OPDs has been widely explored, resulting in solar cells with power conversion efficiency (PCE) exceeding 17%.[14] Tandem OPDs can be made either with two different bandgap materials in the subcells or by stacking two identical subcells. The latter are generally referred to as homo-tandem cells. Here, we show that the higher V_{OC} of homo-tandem OPD pixels over single-junction pixels leads to higher stimulating charge per unit area, thus not sacrificing areal density. Therefore, our approach aims at combining the benefits of organic flexible implants and stimulating microelectrodes, paving the way toward future development of high-resolution retinal prostheses based on soft materials.

First, we characterize the photoresponse of NIR-sensitive single-junction and tandem OPDs based on a polymer–fullerene bulk heterojunction. Second, we investigate the time and voltage dependence of charge storage on stimulating electrodes into a physiological saline solution under pulsed electrical bias. We combine our experimental results to simulate charge accumulation on a stimulating electrode connected to single-junction or tandem OPDs upon pulsed NIR illumination. Assuming scalability of the current–voltage characteristics with the photoactive area, we finally discuss pixel size and light intensity required to achieve efficient neural stimulation.

We developed solution-processed NIR-sensitive OPDs using poly[[2,5-bis(2-hexyldecyl)-2,3,5,6-tetrahydro-3,6-dioxopyrrolo[3,4-c]pyrrole-1,4-diyl]-*alt*-[2,2′:5′,2″-terthiophene]-5,5″-diyl] (PDPP3T) as electron donor in combination with phenyl-C_{61}-butyric acid methyl ester ($PC_{61}BM$) as electron acceptor in the photoactive layer. The deep HOMO of PDPP3T (–5.30 eV)[15] results in relatively high V_{OC}, which is largely determined by the energy difference between HOMO of the donor and LUMO of the acceptor. As a consequence, PDPP3T shows relatively low photon energy loss relative to the optical bandgap (E_g), defined as $E_{loss} = E_g - qV_{OC}$.[16] To increase the V_{OC} under monochromatic lighting conditions even further, we made tandem OPDs with PDPP3T:$PC_{61}BM$ in both subcells (**Figure 2**a). The photoactive layers were connected

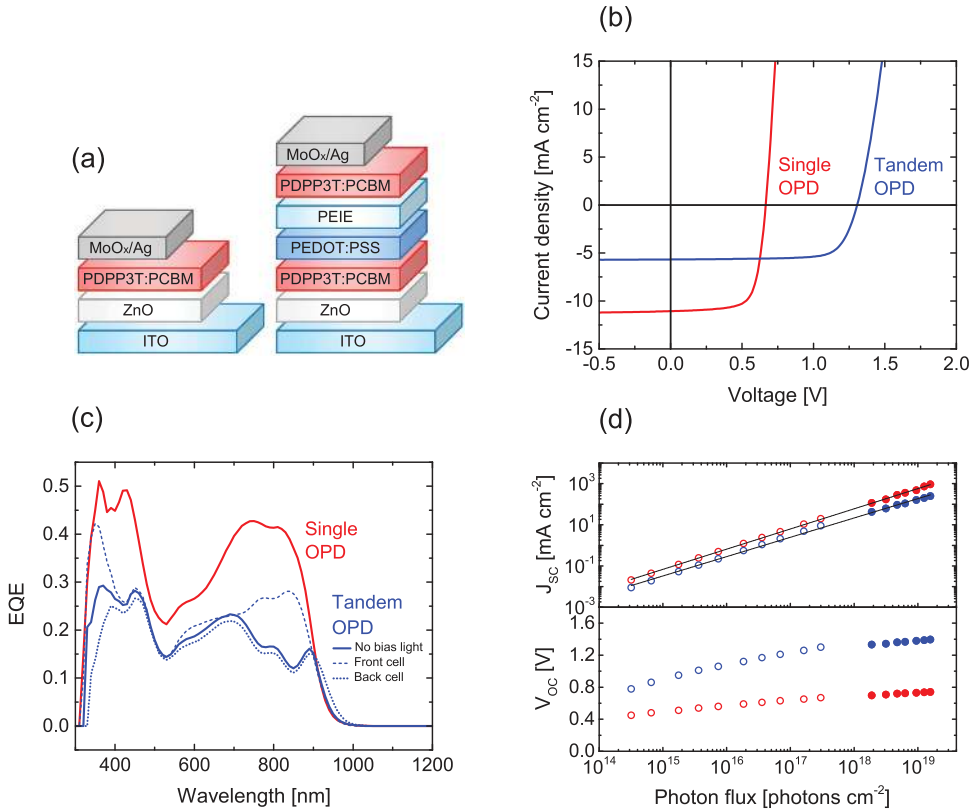

Figure 2. a) Device layout of single-junction (left) and tandem (right) OPD. b) *J–V* characteristics under simulated sunlight (AM1.5G, 100 mW cm^{-2}). c) EQE spectra. For the tandem OPD, 730 and 940 nm light sources were used to optically bias the front and back subcell, respectively. d) Short-circuit current density (J_{SC}) and open-circuit voltage (V_{OC}) as function of photon flux for single-junction (red) and tandem (blue) OPD. Empty and filled markers correspond to data measured under monochromatic 730 and 830 nm illumination, respectively. The solid lines in the upper half of panel (d) represent a power law fit of J_{SC} to photon flux Φ ($J_{SC} \propto \Phi^{\alpha}$). The best fit exponents α are 0.98 (single-junction) and 0.94 (tandem).

in series by a PEDOT:PSS/PEIE interconnecting layer. ZnO was used as electron transporting layer and MoO_x as hole transport layer. The optimal photoactive layer thickness was determined by a combination of optical simulations of the layer stack and experimental current density–voltage (*J–V*) and external quantum efficiency (EQE) measurements of representative single-junction cells (Figure S1, Supporting Information).[17]

Figure 2b shows the *J–V* characteristics of single-junction and tandem OPD under simulated solar light (AM1.5G, 100 mW cm^{-2}). As indicated in **Table 1**, tandem OPDs exhibit approximately double the V_{OC} of single-junction OPDs. The 30 mV loss is mainly a result of the lower light intensity in each of the subcells compared to single-junction diodes.[18] Tandem OPDs show approximately half the short-circuit current density (J_{SC}) of single-junction OPDs under same illumination conditions because two, instead of one, absorbed photons are needed to sustain the photocurrent. An overview of the photovoltaic parameters of 15 tested OPDs is given in Table S1 (Supporting Information).

Table 1. Photovoltaic parameters of single-junction and tandem PDPP3T:$PC_{61}BM$ OPDs under simulated sunlight (AM1.5G, 100 mW cm^{-2}).

OPD	V_{OC} [V]	J_{SC} [mA cm^{-2}]	FF	PCE [%]
Single-junction	0.67	11.1	0.71	5.3
Tandem	1.31	5.67	0.75	5.6

The EQE spectrum of single-junction and tandem OPDs shows NIR sensitivity with an absorption edge at ≈930 nm (Figure 2c). To reproduce the typical lighting conditions for a retinal implant,[19] we measured the photovoltaic parameters under high-intensity monochromatic NIR illumination. Figure 2d shows the V_{OC} and J_{SC} dependence on photon flux for single-junction and tandem OPDs under 730 and 830 nm light. The J_{SC} increases linearly with increasing photon flux over more than four orders of magnitude. V_{OC} approaches 1.4 V for tandem OPDs under 830 nm illumination at ≈1000 mW cm^{-2} (≈5 × 10^{18} photons cm^{-2}). For 830 nm pulsed illumination with 4 ms pulse duration, this light intensity is more than one order of magnitude below the ocular safety limit for peak irradiance.[20]

We investigated the process of charge accumulation on stimulating electrodes into the electrolyte when they are connected to single-junction and tandem OPDs (**Figure 3**a). The OPD converts pulsed NIR light into pulsed photocurrent delivered to the electrode–electrolyte interface. Stimulation current flows from the stimulating electrode to a larger return electrode. We described this system using a previously reported macroscopic equivalent circuit model,[19] where the interface between each electrode and the electrolyte is described by an access resistance R_a in series with a Faradaic impedance, i.e., a double-layer capacitance C with a parallel Faradaic resistance R_F. Quantities with labels 1 and 2 refer to stimulating

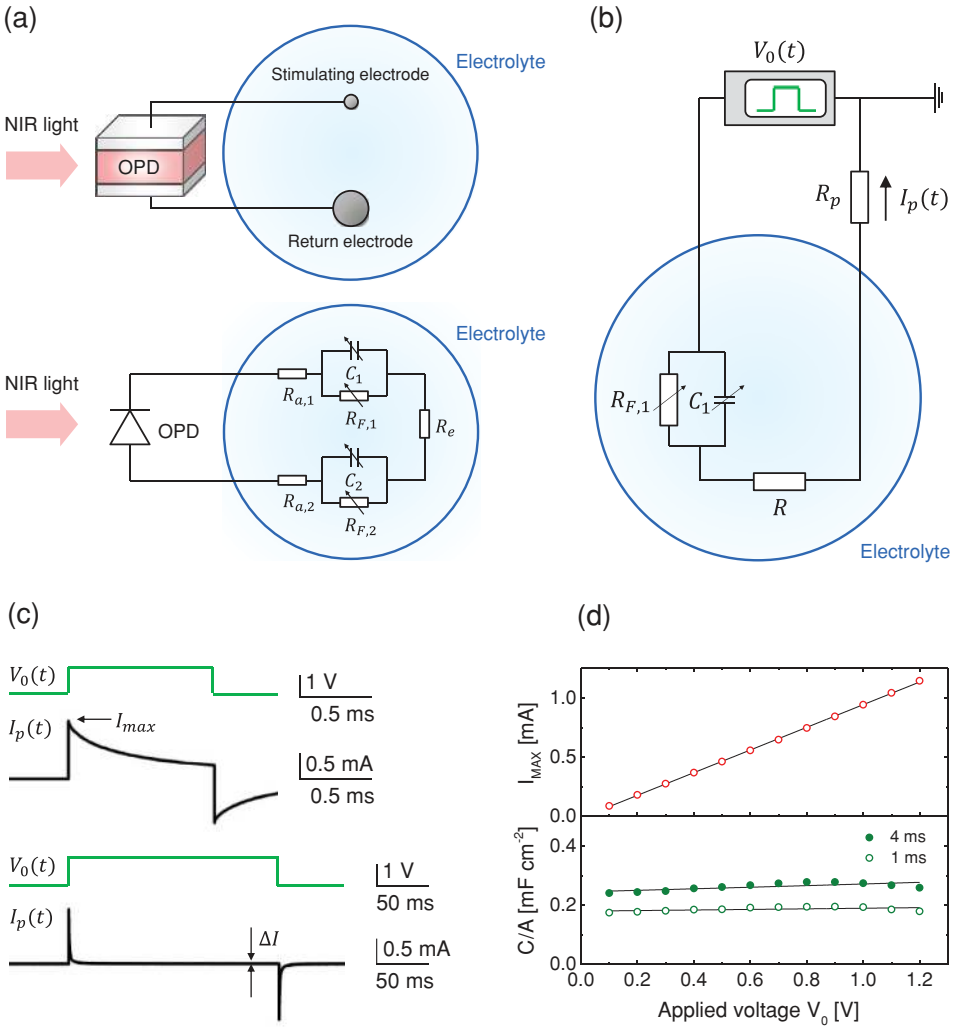

Figure 3. a) Equivalent circuit model of an OPD connected to stimulating and return electrode into an electrolyte solution. R_a is the electrode access resistance, R_F is the Faradaic resistance, C is the double-layer capacitance, and R_e is the electrolyte bulk resistance. Quantities with labels 1 and 2 correspond to stimulating and return electrode, respectively. b) Experimental setup for electrode characterization. Voltage pulses $V_0(t)$ are applied to TiN stimulating electrode and current waveforms $I_p(t)$ through a known probe resistance R_p are monitored. c) Voltage and current waveforms at the electrode–electrolyte interface for 1 and 200 ms pulse duration. d) Maximum current peak I_{max} and double-layer capacitance per unit area C/A as function of applied voltage V_0. The straight lines are linear fits to the experimental data.

and return electrode, respectively. R_e is the electrolyte bulk resistance.

We fabricated stimulating and return electrodes using sputtered titanium nitride (TiN), a widely used material for neural stimulation due to good biocompatibility and high charge injection capacity.[21] Because the TiN electrode properties rely on how they are exactly made, we characterized them to find numerical values of the circuit components in Figure 3a. We applied voltage pulses $V_0(t)$ to 0.275 mm^2 stimulating electrodes in phosphate-buffered saline (PBS) and we analyzed the current waveforms $I_p(t)$ flowing across a known probe resistance R_p (Figure 3b). We used return electrodes with surface area more than ten times larger than the stimulating electrodes. Therefore, we neglected the contribution of the very large capacitance C_2 and Faradaic resistance R_{F2} on the circuit dynamics. In this simplified electrical circuit, the electrolyte and access resistance are combined to a single variable $R = R_e + R_{a,1}$.

The voltage and current waveforms at the electrode–electrolyte interface are shown in Figure 3c for 1 and 200 ms pulse duration. The resistance R is calculated as the ratio between the applied voltage V_0 and the maximum current peak I_{max}, $R = V_0/I_{max}$. The Faradaic resistance is estimated as $R_{F1} = V_0/\Delta I - R \cong V_0/\Delta I$, being ΔI the steady state current flowing at long pulse duration. However, due to negligible ΔI values we disregarded the contribution of R_{F1} on the circuit dynamics. The capacitance at a given pulse duration t is assessed as the ratio between charge and voltage across the double-layer capacitor, $C_1(t) = Q_C(t)/V_C(t)$. The charge $Q_C(t)$ is obtained by integrating the current over time, $Q_C(t) = \int I_p(t)\,dt$. The voltage $V_C(t)$ is given by the Kirchhoff's equation $V_C(t) = V_0(t) - I_p(t)R$.

From the linear fit of I_{max} as function of the applied voltage V_0, $R = 1$ kΩ is found (Figure 3d). For a disk electrode in a conductive medium, we assume the resistance R to scale with the electrode diameter d (≈ 600 µm) according to $R = \rho/2d$, resulting

in electrolyte resistivity $\rho \approx 120\ \Omega$ cm. The TiN capacitance per unit area C/A upon 1 ms voltage pulses reaches about 0.2 mF cm^{-2}, thereby exceeding typical capacitance values for metal electrodes with low surface roughness (≈0.01 mF cm^{-2}).[22] The slight increase in capacitance with voltage pulse duration has been explained as the result of ion diffusion into porous electrode materials, thus resulting in a larger effective surface area.[19]

The time response of organic photovoltaic cells to pulsed illumination shows that they behave as almost ideal power sources that switch from an active power generating state to a passive power consuming state on the timescale of a microsecond.[23] Furthermore, the capacitance of the photovoltaic cells is small in comparison with the capacitances of the stimulating electrodes used in this work. These conditions allow for reliable calculation of the electrical charge generated by OPD micropixels coupled to TiN stimulating microelectrodes under pulsed illumination. We assumed appropriate area scaling of the OPD current density and the TiN electrode double-layer capacitance per unit area C/A. As an example, **Figure 4**a shows the I–V characteristics for a 2500 μm^2 OPD pixel in dark and under 1500 mW cm^{-2} 830 nm illumination (black and red) and the electrolyte load lines for a 40 μm diameter TiN disk electrode into an electrolyte with resistivity corresponding to the retinal tissue ($\rho \approx 1000\ \Omega$cm)[24] in case of discharged (dotted blue) and charged (dotted orange) electrode.

The OPD characteristics and the load line are used to calculate the time response of the current in saline solution upon pulsed illumination (Figure 4b). When illumination is off, no current is generated by the OPD (point 1). As the light pulse is applied, the OPD current is given by the intersection between the I–V characteristic and the load line (point 2). During the light pulse the TiN electrode is charged, shifting the load line by an amount equal to the voltage across the double-layer capacitor. In this step, the system evolves toward point 3 and the current transient is calculated by solving the following system of equations:

$$\begin{cases} I = +I_{SC} - I_0\left[\exp\left(\dfrac{qV}{nkT}\right) - 1\right] \\ I = \dfrac{V - V_{\text{cap}}(t)}{R} \end{cases} \tag{1}$$

where the first equation is used to fit the I–V characteristics under illumination and the second equation describes the load line in case of charged electrode, being $V_{\text{cap}}(t) = \dfrac{1}{C}\int I(t)\,dt$ the time-dependent voltage across the electrode capacitor. To solve this system, we find the voltage V at each time step by numerically integrating the current over time. When the light pulse is turned off, the system switches to point 4 resulting in a current of opposite polarity flowing through the resistance R. Finally, the OPD discharges with time to reach the initial state (point 1). In this step, we compute the current solving system (1) with $I_{SC} = 0$. We calculate the charge per pulse Q by integrating the positive current waveform over the pulse duration t_1:

$$Q = \int_0^{t_1} I(t)\,dt \tag{2}$$

Figure 4c shows the charge per pulse as function of light intensity for a 2500 μm^2 single-junction and tandem OPD pixel coupled to a 40 μm diameter TiN disk electrode upon 4 ms pulsed illumination. The neural stimulation window for microelectrodes lies in a narrow range of Q values between 1 and 4 nC, as determined by the tissue functional threshold and the tissue damage threshold, respectively.[25] At low light intensities, the charge per pulse increases linearly with light intensity. Here, the microelectrode charging is current limited, as the load line intersects the I–V characteristic close to the short-circuit current (I_{SC}) throughout the pulse duration. Under these conditions, higher charge values are reached with single-junction OPD due to the higher I_{SC}. However, at higher light intensities the current pulses are voltage-limited as the OPD reaches the V_{OC} during the light pulse. Here, the charge quickly saturates with light intensity and the tandem OPD outperforms the single-junction due to the higher V_{OC}.

Both single-junction and tandem OPD pixels can deliver the required charge to stimulate neurons under pulsed NIR illumination at intensities < 100 mW cm^{-2}, thus more than two orders of magnitude below the ocular safety limit for 4 ms pulsed illumination. However, for the optimal operation of a retinal implant, a linear response between charge and light intensity in the aforementioned narrow neural stimulation window is a prerequisite. This linear response allows for precise tuning of the brightness of the restored image. As it can be seen in Figure 4c, only tandem OPD pixels can linearly tune the charge throughout the neural stimulation window.

To efficiently convert pulsed illumination into stimulating photogenerated charge at video rate (20 Hz), complete electrode discharge between the light pulses is desirable. Residual charge accumulated on the electrodes would result in a decrease of current upon consecutive light pulses.[19] The calculated residual current is still ≈1% of the maximum current after 50 ms (Figure 4d), thus resulting in lower photogenerated charge upon the following light pulse (Figure S3, Supporting Information). We investigated the electrode discharge rate for tandem OPDs with smaller shunt resistance, causing a higher leakage current density (Figure S4, Supporting Information), but with comparable photovoltaic performance (Table S1, Supporting Information). However, the discharge is not faster for high leakage tandem OPDs during the first 50 ms after the light pulse due to the lower conductance close to the load line intersection. Only beyond 600 ms the residual charge is lower for high leakage tandem OPDs due to the higher conductance at low voltages. Residual charge accumulation might be reduced by adding a shunt resistor to accelerate the electrode discharge rate.[26] In this respect, we note that for the envisioned OPD application in retinal implants operated without external bias the dark current is much less relevant than for imaging applications. For the latter, low dark currents in reverse bias are required to improve the device sensitivity. For the present tandem OPDs, the dark leakage current is on the order of 10^{-4} mA cm^{-2} at –2 V.

Figure 4e,f shows the superior performance of tandem OPD pixels over single-junction pixels for several combinations of photoactive area and stimulating electrode size. Tandem OPD pixels with photoactive area from 2500 to 6250 μm^2 and electrode

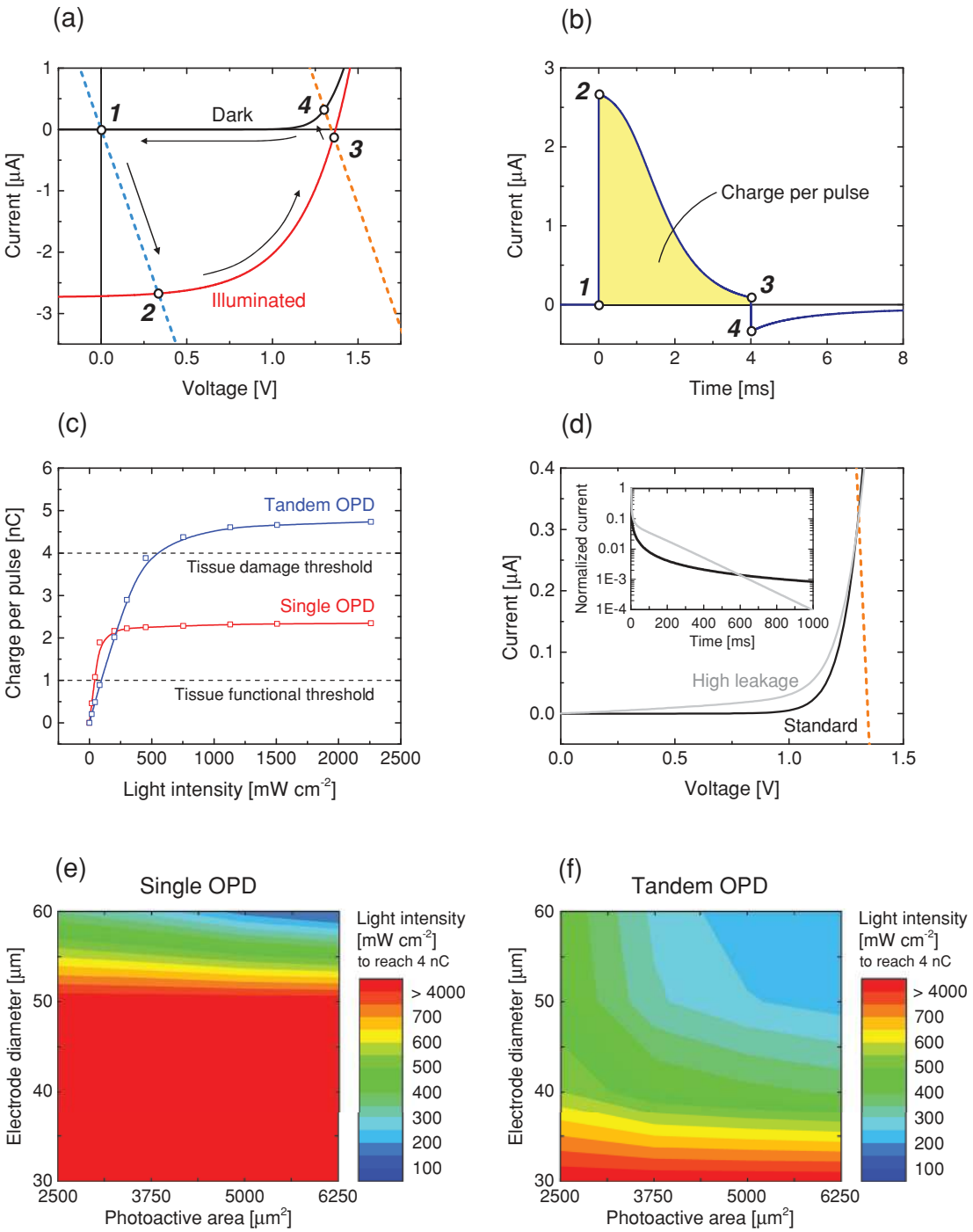

Figure 4. a) *I–V* characteristics for a 2500 µm^2 tandem OPD pixel in dark (black) and under 1500 mW cm^{-2} 830 nm illumination (red); electrolyte load line for 40 µm diameter TiN disk electrode in a 1000 Ωcm resistivity medium in case of discharged (dotted blue) and charged (dotted orange) electrode. b) Reconstruction of current waveform upon 4 ms pulsed illumination. Charge per pulse *Q* is calculated by integrating the current transient over time. c) Charge per pulse as function of light intensity for single-junction and tandem OPD micropixels. Solid lines are guides to the eyes. The charge damage threshold (4 nC) limits the maximum applicable light intensity to ≈ 600 mW cm^{-2} for tandem OPD pixels. The curves up to 2500 mW cm^{-2} show the linear-to-logarithmic transition of the charge per pulse discussed in the text. d) Current transient during discharge for standard (black) and high leakage (gray) tandem OPD pixel. e,f) Design rules to cover the entire charge per pulse stimulation window (≈4 nC) upon 4 ms light pulse using single-junction and tandem OPD pixels.

diameter down to ≈35 µm can efficiently tune *Q* throughout the neural stimulation window upon 4 ms light pulse at physiologically safe intensity (from 150 to 600 mW cm^{-2}). Instead, single-junction OPD pixels with the same geometry would require intensities beyond the range used in this study (>4000 mW cm^{-2}). Stimulation with single-junction OPD pixels

at lower light intensity is only possible with 60 µm diameter electrodes. However, this would result in a larger overall pixel dimension, thereby reducing the implant resolution.

In summary, we investigated NIR-sensitive OPDs as photovoltaic pixels in an artificial retinal implant. We fabricated and characterized solution-processed single-junction and tandem OPDs as well as sputtered TiN stimulating electrodes. Combining our experimental results, we simulated the performance of OPD micropixels coupled to TiN microelectrode in a physiological environment upon pulsed NIR illumination. The higher V_{OC} of tandem OPD pixels over single-junction pixels maximizes charge accumulation on the stimulating microelectrode. Tandem OPD pixels with small electrode size (≈35 µm in diameter) can cover the entire charge per pulse neural stimulation window at physiologically safe light intensities. This opens a way toward future development of high-resolution retinal prostheses based on flexible OPD arrays.

Experimental Section

Single-Junction and Tandem OPDs: Device fabrication and characterization was performed according to recently published methods[27] and is further detailed in Supporting Information.

Stimulating and Return Electrodes: TiN electrodes were deposited on glass substrates by sputtering. The stimulating and return electrode geometrical surface areas were defined upon application of insulating Kapton tape by 0.275 and 10 mm^2 apertures, respectively. The electrodes were then placed in PBS (0.01 M phosphate buffer, 2.7×10^{-3} M KCl, and 137×10^{-3} M NaCl, pH 7.4) from Sigma-Aldrich. 1 and 200 ms voltage pulses from 0.1 to 1.3 V in 0.1 steps were applied by a pulse generator. A 100 Ω probe resistance R_p was used to analyze the current waveforms at the electrode–electrolyte interface.

Supporting Information

Supporting Information is available from the Wiley Online Library or from the author.

Acknowledgements

The authors thank Dario Simone for his contribution to this work. The research received funding from the Ministry of Education, Culture and Science (Gravity program 024.001.035) and the European Research Council under the European Union's Seventh Framework Programme (FP/2007-2013)/ERC Grant Agreement No. 339031.

Conflict of Interest

The authors declare no conflict of interest.

Keywords

bulk heterojunctions, neural stimulation, organic photovoltaics, retinas, tandem cells

Received: July 21, 2018
Revised: August 30, 2018
Published online: October 15, 2018

[1] D. T. Hartong, E. L. Berson, T. P. Dryja, *Lancet* **2006**, *368*, 1795.
[2] N. M. Bressler, S. B. Bressler, S. L. Fine, *Surv. Ophthalmol.* **1988**, *32*, 375.
[3] L. da Cruz, B. F. Coley, J. Dorn, F. Merlini, E. Filley, P. Christopher, F. K. Chen, V. Wuyyuru, J. Sahel, P. Stanga, M. Humayun, R. J. Greenberg, G. Dagnelie, *Br. J. Ophthalmol.* **2013**, *97*, 632.
[4] E. Zrenner, K. U. Bartz-Schmidt, H. Benav, D. Besch, A. Bruckmann, V. P. Gabel, F. Gekeler, U. Greppmaier, A. Harscher, S. Kibbel, J. Koch, A. Kusnyerik, T. Peters, K. Stingl, H. Sachs, A. Stett, P. Szurman, B. Wilhelm, R. Wilke, *Proc. R. Soc. B* **2011**, *278*, 1489.
[5] K. Mathieson, J. Loudin, G. Goetz, P. Huie, L. Wang, T. I. Kamins, L. Galambos, R. Smith, J. S. Harris, A. Sher, D. Palanker, *Nat. Photonics* **2012**, *6*, 391.
[6] H. Lorach, G. Goetz, R. Smith, X. Lei, Y. Mandel, T. Kamins, K. Mathieson, P. Huie, J. Harris, A. Sher, D. Palanker, *Nat. Med.* **2015**, *21*, 476.
[7] D. Ghezzi, M. R. Antognazza, M. Dal Maschio, E. Lanzarini, F. Benfenati, G. Lanzani, *Nat. Commun.* **2011**, *2*, 166.
[8] D. Ghezzi, M. R. Antognazza, R. Maccarone, S. Bellani, E. Lanzarini, N. Martino, M. Mete, G. Pertile, S. Bisti, G. Lanzani, F. Benfenati, *Nat. Photonics* **2013**, *7*, 400.
[9] J. F. Maya-Vetencourt, D. Ghezzi, M. R. Antognazza, E. Colombo, M. Mete, P. Feyen, A. Desii, A. Buschiazzo, M. Di Paolo, S. Di Marco, F. Ticconi, L. Emionite, D. Shmal, C. Marini, I. Donelli, G. Freddi, R. Maccarone, S. Bisti, G. Sambuceti, G. Pertile, G. Lanzani, F. Benfenati, *Nat. Mater.* **2017**, *16*, 681.
[10] T. Flores, G. Goetz, X. Lei, D. Palanker, *J. Neural Eng.* **2016**, *13*, 036010.
[11] L. Wang, K. Mathieson, T. I. Kamins, J. D. Loudin, L. Galambos, G. Goetz, A. Sher, Y. Mandel, P. Huie, D. Lavinsky, J. S. Harris, D. V. Palanker, *J. Neural Eng.* **2012**, *9*, 046014.
[12] G. H. Gelinck, A. Kumar, D. Moet, J. L. P. J. van der Steen, A. J. J. M. van Breemen, S. Shanmugam, A. Langen, J. Gilot, P. Groen, R. Andriessen, M. Simon, W. Ruetten, A. U. Douglas, R. Raaijmakers, P. E. Malinowski, K. Myny, *IEEE Trans. Electron Devices* **2016**, *63*, 197.
[13] F. Arca, M. Sramek, S. F. Tedde, P. Lugli, O. Hayden, *IEEE J. Quantum Electron.* **2013**, *49*, 1016.
[14] L. Meng, Y. Zhang, X. Wan, C. Li, X. Zhang, Y. Wang, X. Ke, Z. Xiao, L. Ding, R. Xia, H.-L. Yip, Y. Cao, Y. Chen, *Science* **2018**, *361*, 1094.
[15] K. H. Hendriks, G. H. L. Heintges, V. S. Gevaerts, M. M. Wienk, R. A. J. Janssen, *Angew. Chem., Int. Ed.* **2013**, *52*, 8341.
[16] W. Li, K. H. Hendriks, A. Furlan, M. M. Wienk, R. A. J. Janssen, *J. Am. Chem. Soc.* **2015**, *137*, 2231.
[17] J. Gilot, M. M. Wienk, R. A. J. Janssen, *Adv. Mater.* **2010**, *22*, E67.
[18] D. Di Carlo Rasi, K. H. Hendriks, M. M. Wienk, R. A. J. Janssen, *Adv. Energy Mater.* **2017**, *7*, 1701664.
[19] D. Boinagrov, X. Lei, G. Goetz, T. I. Kamins, K. Mathieson, L. Galambos, J. S. Harris, D. Palanker, *IEEE Trans. Biomed. Circuits Syst.* **2016**, *10*, 85.
[20] F. C. Delori, R. H. Webb, D. H. Sliney, *J. Opt. Soc. Am. A* **2007**, *24*, 1250.
[21] S. F. Cogan, *Annu. Rev. Biomed. Eng.* **2008**, *10*, 275.
[22] D. Palanker, A. Vankov, P. Huie, S. Baccus, *J. Neural Eng.* **2005**, *2*, S105.
[23] D. Credgington, J. R. Durrant, *J. Phys. Chem. Lett.* **2012**, *3*, 1465.
[24] C. J. Karwoski, D. A. Frambach, L. M. Proenza, *J. Neurophysiol.* **1985**, *54*, 1607.
[25] S. F. Cogan, presented at the 26th Annual Int Conf. of the IEEE EMBS San Francisco, CA, September **2004**.
[26] J. D. Loudin, S. F. Cogan, K. Mathieson, A. Sher, D. V. Palanker, *IEEE Trans. Biomed. Circuits Syst.* **2011**, *5*, 468.
[27] D. Di Carlo Rasi, K. H. Hendriks, G. H. L. Heintges, G. Simone, G. H. Gelinck, V. S. Gevaerts, R. Andriessen, G. Pirotte, W. Maes, W. Li, M. M. Wienk, R. A. J. Janssen, *Sol. RRL* **2018**, *2*, 1800018.